Geophysical Research Letters

RESEARCH LETTER
10.1029/2022GL100747

Key Points:

- Water ice is exposed in a 150 m-diameter new impact crater near 35°N on Mars
- The ice includes both massive ice and a covering layer of pore ice
- This ice marks the southern margin of remaining ice deposits from high-obliquity periods

Supporting Information:

Supporting Information may be found in the online version of this article.

Correspondence to:

C. M. Dundas,
cdundas@usgs.gov

Citation:

Dundas, C. M., Mellon, M. T., Posiolova, L. V., Miljković, K., Collins, G. S., Tornabene, L. L., et al. (2023). A large new crater exposes the limits of water ice on Mars. *Geophysical Research Letters*, *50*, e2022GL100747. https://doi.org/10.1029/2022GL100747

Received 16 AUG 2022
Accepted 18 NOV 2022

Author Contributions:

Conceptualization: Colin M. Dundas, Michael T. Mellon, Liliya V. Posiolova, Shane Byrne, Alfred S. McEwen, Gunnar Speth
Formal analysis: Colin M. Dundas, Michael T. Mellon, Katarina Miljković, Gareth S. Collins, Livio L. Tornabene, Vidhya Ganesh Rangarajan, Kimberly D. Seelos

A Large New Crater Exposes the Limits of Water Ice on Mars

Colin M. Dundas[1], Michael T. Mellon[2], Liliya V. Posiolova[3], Katarina Miljković[4], Gareth S. Collins[5], Livio L. Tornabene[6], Vidhya Ganesh Rangarajan[6], Matthew P. Golombek[7], Nicholas H. Warner[8], Ingrid J. Daubar[9], Shane Byrne[10], Alfred S. McEwen[10], Kimberly D. Seelos[11], Donna Viola[12], Ali M. Bramson[13], and Gunnar Speth[3]

[1]Astrogeology Science Center, U. S. Geological Survey, Flagstaff, AZ, USA, [2]Cornell University, Ithaca, NY, USA, [3]Malin Space Science Systems, San Diego, CA, USA, [4]School of Earth and Planetary Sciences, Space Science and Technology Centre, Curtin University, Perth, WA, Australia, [5]Department of Earth Science and Engineering, Imperial College London, London, UK, [6]Department Earth Science, Institute for Earth & Space Exploration, University of Western Ontario, London, ON, Canada, [7]Jet Propulsion Laboratory, California Institute of Technology, Pasadena, CA, USA, [8]SUNY Geneseo, Geneseo, NY, USA, [9]Brown University, Providence, RI, USA, [10]Lunar and Planetary Laboratory, The University of Arizona, Tucson, AZ, USA, [11]Johns Hopkins University Applied Physics Laboratory, Laurel, MD, USA, [12]KBR, Inc., Sioux Falls, SD, USA, [13]Department of Earth, Atmospheric, and Planetary Sciences, Purdue University, West Lafayette, IN, USA

Abstract Water ice in the Martian mid-latitudes has advanced and retreated in response to variations in the planet's orbit, obliquity, and climate. A 150 m-diameter new impact crater near 35°N provides the lowest-latitude impact exposure of subsurface ice on Mars. This is the largest known ice-exposing crater and provides key constraints on Martian climate history. This crater indicates a regional, relatively pure ice deposit that is unstable and has nearly vanished. In the past, this deposit may have been tens of meters thick and extended equatorward of 35°N. We infer that it is overlain by pore ice emplaced during temporary stable intervals, due to recent climate variability. The marginal survival of ice here suggests that it is near the edge of shallow ice that regularly exchanges with the atmosphere.

Plain Language Summary A 150 m-diameter new impact crater on Mars exposes water ice, constraining the nature of past and present ice sheets and paleoclimate. The past climate has varied, gradually removing a massive ice deposit that has nearly been lost at 35°N but survives at higher latitude.

1. Introduction

The mid-latitudes are critical for understanding the recent climate of Mars. Temperature and atmospheric water vapor control subsurface water ice stability (e.g., Chamberlain & Boynton, 2007; Mellon & Jakosky, 1995; Mellon et al., 2004), with colder temperatures and higher humidity causing shallower ice. Shallow ice is ubiquitous at high latitudes (e.g., Boynton et al., 2002; Smith et al., 2009) and stable at depths of centimeters (e.g., Mellon et al., 2004). At mid-latitudes warmer temperatures increase the depth of stable ice to as much as a few meters. Further equatorward, ice is absent or buried deeply enough to persist while sublimating, or localized on pole-facing slopes (e.g., Aharonson & Schorghofer, 2006).

Variations in the orbit and obliquity of Mars affect temperature and humidity, causing ice to extend equatorward as obliquity increases and retreat as it decreases (e.g., Chamberlain & Boynton, 2007; Mellon & Jakosky, 1995; Mellon & Sizemore, 2022; Schorghofer, 2007; Schorghofer & Forget, 2012). Past snow and frost accumulation have produced mid-latitude glaciers and decameters-thick, relatively pure regional ice deposits (e.g., Bramson et al., 2015; Holt et al., 2008). Paleoclimate models suggest that such deposition is favored at an obliquity near 35°, compared with the present 25.19° (e.g., Madeleine et al., 2009, 2014; Mischna et al., 2003). The obliquity of Mars varies widely and regularly exceeded 30° prior to 380 ka (Laskar et al., 2004). The distribution of mid-latitude ice on Mars reflects the history of deposition and removal following these controls. Thus, finding the lowest-latitude shallow ice is an important constraint on the climate history, in addition to being of significant interest as a target for future exploration.

The Mars Reconnaissance Orbiter Context Camera (CTX; Malin et al., 2007) imaged a 150 ± 10-m-diameter new impact crater at 35.1°N, 189.8°E that formed 24 December 2021 (Posiolova et al., 2022). The crater was imaged by the High Resolution Imaging Science Experiment (HiRISE; McEwen et al., 2007) on 27 February 2022 (Figures 1a and 1b). Bright patches and blocks indicate that this impact excavated ice, like other mid-latitude

Funding acquisition: Katarina Miljković, Gareth S. Collins, Ingrid J. Daubar, Shane Byrne, Alfred S. McEwen
Investigation: Colin M. Dundas, Michael T. Mellon, Katarina Miljković, Gareth S. Collins, Livio L. Tornabene, Vidhya Ganesh Rangarajan, Matthew P. Golombek, Nicholas H. Warner, Ingrid J. Daubar, Shane Byrne, Alfred S. McEwen, Kimberly D. Seelos, Donna Viola, Ali M. Bramson, Gunnar Speth
Methodology: Colin M. Dundas, Katarina Miljković, Gareth S. Collins, Livio L. Tornabene, Vidhya Ganesh Rangarajan, Nicholas H. Warner, Kimberly D. Seelos
Project Administration: Shane Byrne, Alfred S. McEwen
Resources: Colin M. Dundas
Visualization: Colin M. Dundas, Katarina Miljković, Gareth S. Collins, Nicholas H. Warner, Kimberly D. Seelos, Ali M. Bramson
Writing – original draft: Colin M. Dundas, Katarina Miljković, Gareth S. Collins, Livio L. Tornabene, Vidhya Ganesh Rangarajan
Writing – review & editing: Colin M. Dundas, Michael T. Mellon, Liliya V. Posiolova, Katarina Miljković, Gareth S. Collins, Livio L. Tornabene, Vidhya Ganesh Rangarajan, Matthew P. Golombek, Nicholas H. Warner, Ingrid J. Daubar, Shane Byrne, Alfred S. McEwen, Kimberly D. Seelos, Donna Viola, Ali M. Bramson

craters (Dundas et al., 2021) but at lower latitude and in a larger and deeper crater than any previous known impact exposure. Observations of this crater enable us to establish the properties of the ice table and regional history in more detail than previous crater exposures.

2. Observations

Bright material around the crater at 35.1°N, 189.8°E is consistent with water ice. A near-infrared spectrum from the Compact Reconnaissance Imaging Spectrometer for Mars (CRISM; Murchie et al., 2007) is consistent with water ice (Figure S1, Text S1 in Supporting Information S1). A ratio of putative ice-bearing material in the CRISM data (3 pixel mean) was made to similar albedo material within the same detector columns (26 pixel mean) 3.1 km away and shows a 1.02 μm wavelength absorption feature indicative of water ice. It meets geomorphic criteria for ice-exposing impacts (Dundas et al., 2021): it is blue-to-white in HiRISE relative color, substantially brighter than the surroundings (not merely distinct in color), and very distinct from other ejecta material, implying a distinct composition. A second large new crater at 38.1°N, 280.1°E (Posiolova et al., 2022) also has possible ice (Figure S2 in Supporting Information S1) but is not as well supported and not discussed further here.

The crater cavity contains little visible ice, unlike some higher-latitude impacts (Dundas et al., 2021). The most prominent ice within the crater was shadowed at the time of imaging but is visible with enhanced contrast (Figure 1c). Bright patches and blocks (up to 3 m diameter; Figure 1b) with icy coloration occur on the proximal ejecta, indicating that the impact excavated ice that is at least ∼3 m thick in places. This bright material must be massive ice with a low lithic content. Pore-filling ice, which may also be present, accumulates an opaque lag within days of exposure (Smith et al., 2009) and would not be apparent in images weeks after impact. The bright patches (Figure 1b) shrank in a second HiRISE image acquired 39 days later, further supporting an interpretation of ice that sublimes when exposed. Ice blocks are visible as far as 700 m from the crater rim. A large fraction of resolved blocks have icy coloration, indicating that massive ice comprises much of the strongest subsurface material, but most of the non-block ejecta lacks such coloration. The primary crater is surrounded by thousands of secondary craters. A few of these craters display bright ice (Figures 1d–1h). The ice is mostly on the crater wall facing the primary, suggesting that it derives from the secondary impactor, and can be seen >8 km from the primary crater.

Some of the larger secondary craters have flat floors (Figures 1d, 1f, and 1g). This morphology is characteristic of excavation to a resistant layer (e.g., Bart, 2014; Quaide & Oberbeck, 1968). Resulting morphologies include flat, terraced, or dimpled floors. Subsurface ice produces a marked strength contrast in otherwise loose regolith and flat-floored craters have been used to infer the ice table depth at other ice-exposing impacts (Dundas et al., 2021). We examined all craters >5 m diameter in HiRISE image ESP_073077_2155 and noted their diameters. We also noted the diameter of a flat floor or other resistant morphology if present. If uncertain, craters were treated as not having a resistant layer. We cannot definitively establish the secondary origin of every crater as most lack bright ice, but based on the appearance of parts of the image far from the new primary crater that were clearly not affected by secondaries we infer that this area had almost no distinct pre-existing craters. However, even if some of the craters included here are not secondaries, their geometry still indicates the depth to a resistant layer.

We used the crater measurements to determine depths to a resistant layer using a relationship between crater diameter, flat floor diameter, and depths to the layer based on experiments (Bart, 2014). We assume an angle of repose of 33°, typical of the angle of internal friction for regolith at various Mars landing sites (Shaw et al., 2009). The mean depth to the resistant layer is 0.97 ± 0.25 m. This standard deviation describes the variation of the results, not possible measurement error. One-pixel errors in opposing directions for rim diameter and flat floor diameter would change depth estimates by 0.15 m. An angle of repose of 30° would reduce estimated depths by 12% and an angle of 38° would increase them by 17%; this range includes angles of internal friction for most materials at Mars landing sites (Shaw et al., 2009).

For craters with no indication of a resistant layer, we estimate the lack of such a layer to a depth of either 0.2× or 0.1× the crater diameter. The first assumption is an approximation based on the occurrence of flat floors beginning with resistant layers at a depth 0.25× the crater diameter or shallower (e.g., Bart, 2014), reduced by 0.05 as marginal cases would not be noticeable. Our second estimate halves this depth because secondary craters are typically shallower than primary craters of the same diameter (Pike & Wilhelms, 1978). Shadow measurements of the largest secondaries without flat floors suggest depth/diameter ratios comparable to small primary craters

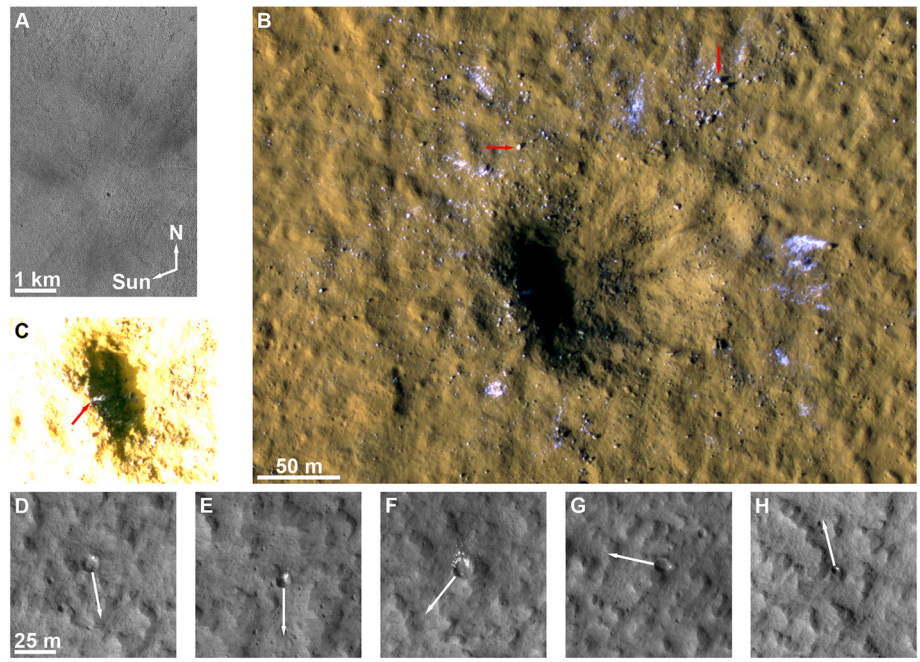

Figure 1. New water ice-exposing crater on Mars. (a) High Resolution Imaging Science Experiment overview showing blast pattern. (b) Enhanced-color image. Excavated material includes icy blocks (red arrows show examples) and larger icy patches in blue-white. (c) A hard contrast stretch of the shadow inside the crater, revealing ice (red arrow). (d–h) Secondary craters with bright ice. White arrows indicate direction to primary crater. The ice is usually concentrated on the down-range side. (d, f, and g) show flat floors. Note also pre-impact hummocky texture. See Text S3 and Table S1 in Supporting Information S1 for image details.

but the reason for this is not understood so we present both assumptions. Results for both assumptions are shown in Figure 2.

The flat floors indicate a resistant layer at ~1 m depth. However, other craters lack flat floors, indicating no strength contrast at the same depths for either depth assumption (Figure 2), so the depth to the resistant layer is variable over the ~65 km^2 examined. The flat floors are not bright, consistent with pore ice or some other resistant material.

3. Modeling

To assess the origin depth of the excavated massive ice, we simulated the formation of the primary crater using the iSALE2D shock physics code (Collins et al., 2004; Wünnemann et al., 2006). Numerical impact modeling was performed using a 180-ton impactor (5 m in diameter) striking the surface of Mars at 12 km/s vertical impact velocity (Text S2 in Supporting Information S1). In this work and Posiolova et al. (2022), as preliminary modeling, we assumed a vertical impact and a homogeneous target with the properties of weak, porous, fractured basalt of bulk density 2,100 kg/m^3 (25% bulk porosity). This material model was used in previous work for simulating small impacts on Mars (Rajšić et al., 2021). Other model parameters are given in Supporting Information S1.

The simulation produces a 128-m-diameter crater with a smooth rim that did not undergo collapse and a rim-to-floor depth of 33 m. This simulated crater is deeper and slightly smaller in diameter than the observed crater (~21 m deep), which may have experienced minor rim collapse, which could result in a slight (~15%) underprediction of excavation depths. Different impact parameters would not affect the first-order results here; a broader, shallower crater is likely if strong ice at depth and weaker, lower density regolith near the surface were included in the model, and (or) with oblique impact effects.

The provenance and state of proximal ejecta were tracked with Lagrangian tracer particles that follow points in the material during the impact and cratering flow (e.g., Pierazzo et al., 1997). Figure 3a shows the depth of origin of crater materials in the final crater structure. Most of the ice deposits are in the continuous ejecta between 75

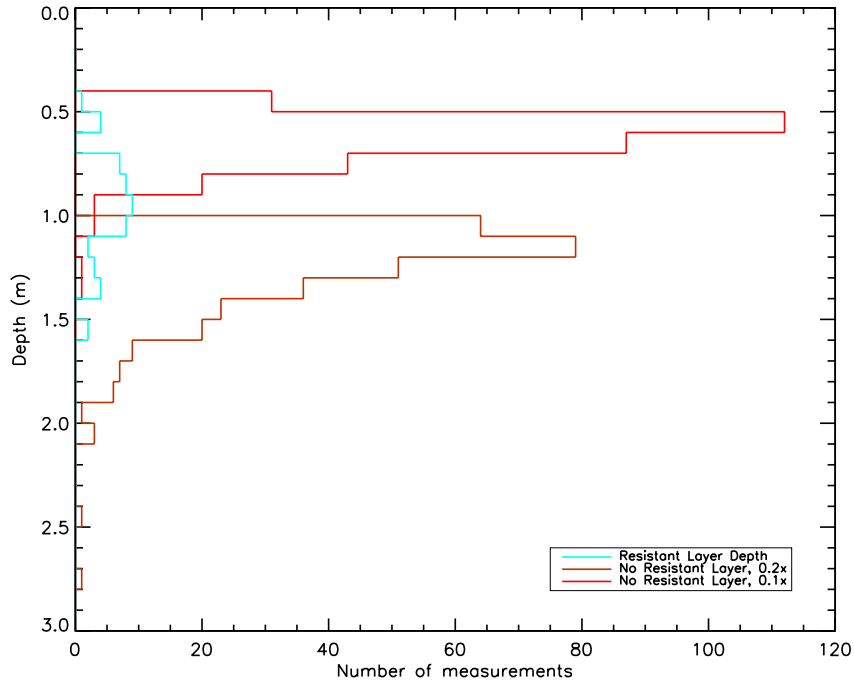

Figure 2. Histogram of resistant layer depths and non-detections. Depths to a resistant layer interpreted to be the ice table are shown in cyan, and depths where a resistant layer does not exist are shown in red for two different assumptions about the depth implied by a given crater diameter. The resistant layer depth has substantial variability and overlaps with depths of non-detections for either assumption, suggesting a variable depth to the layer.

and 140 m from the crater center. The excavation depth of this ejecta is <8 m. Most of the ejecta would have been minimally heated (Figure 3b; Figure S3 and S4 in Supporting Information S1); only about 15% of the continuous ejecta experienced a peak temperature exceeding 273 K and <5% experienced a peak temperature exceeding

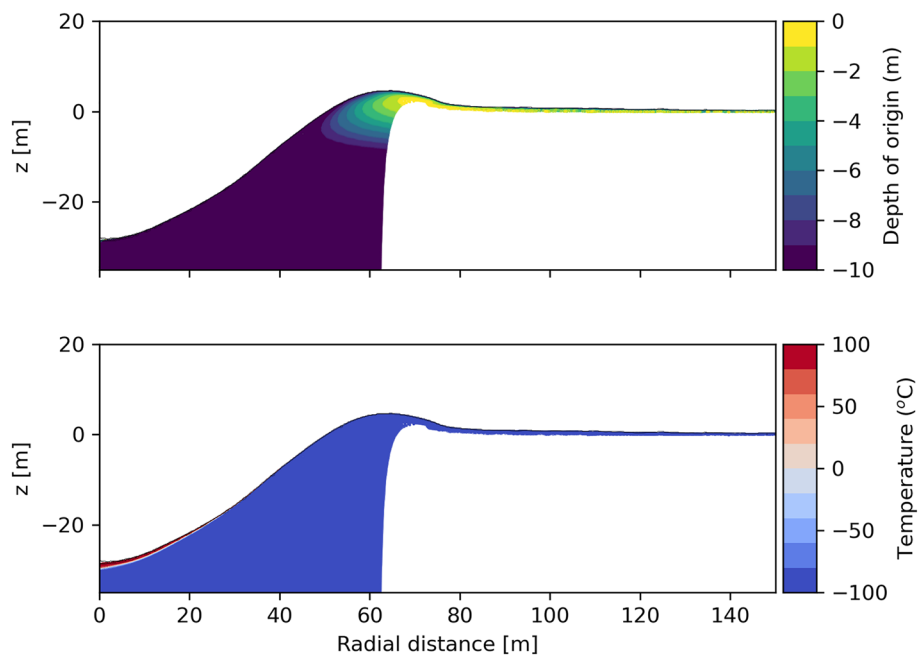

Figure 3. Hydrocode model results. Final crater produced by vertical impact simulations in a homogeneous, porous basaltic target showing depth of origin (a) and peak temperature (b) of material ejected by the impact that lands within 150 m of the impact point.

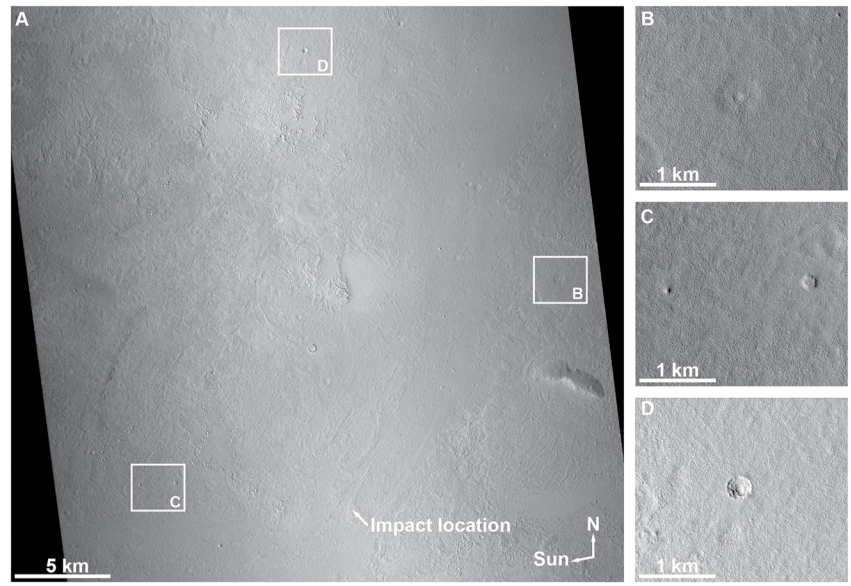

Figure 4. Geomorphology in the vicinity of the impact. (a) Pre-impact image showing rough texture. (b) Expanded crater. (c) Mounds interpreted as crater fill inverted by sublimation (Figure S9 in Supporting Information S1). (d) Terraced crater. See Text S3 and Table S1 in Supporting Information S1 for image details.

373 K. More distal ejecta including blocks hundreds of meters away derives from shallower depths. Thus, the minimum depth to the massive ice is less than 5 m and perhaps as shallow as 2 m. The large ice blocks indicate that some ice did not experience shock pressure greater than the compressive strength of intact ice (~10 MPa; Durham et al., 1983).

4. Regional Context

The region is mapped as young (Late Amazonian) flood lavas (Tanaka et al., 2014). Nearby images reveal a sparsely cratered hummocky-textured coating of mid-latitude mantling deposits (e.g., Kreslavsky & Head, 2002) over the lava (Figure 4). This coating extends to 33°–34°N but is replaced by well-defined platy-ridged lava (cf., Keszthelyi et al., 2008) further south (Figure S5 in Supporting Information S1). Near the impact, rocky ejecta occurs in craters with diameter >500 m but not <60 m (Figures S6 and S7 in Supporting Information S1). Using depth to excavation relationships for material in the continuous ejecta of primary impacts (Melosh, 1989), these craters excavated blocky material from depths >40 m but not from <7 m, so the coating is locally at least 7 and up to 40 m thick. These blocks are rock, as ice blocks around mid-latitude craters sublimate on timescales of years (Dundas et al., 2014).

The new crater is nearly due south of ice-exposing craters at 39.1°N (the previous lowest-latitude such craters) where flat floors indicated an ice-table depth of ~0.9 m (Dundas et al., 2021). It is within 120 km of radar reflectors inferred to indicate decameters-thick massive ice (Bramson et al., 2015), that extend from ~38° to 52°N (Figure S8 in Supporting Information S1). A terraced crater 20 km north (Figure 4d) resembles those used to infer the depth of radar reflectors interpreted as the base of ice in that unit (Bramson et al., 2015).

The surface near the new crater has a hummocky texture (Figures 1 and 4a) and several expanded craters (Figure 4b) as well as isolated mounds (Figure 4c). The hummocky texture likely represents residual regolith after partial ice loss. Modeling suggests that expanded craters form via sublimation of massive ice causing slope retreat around a crater (Dundas et al., 2015). The new crater is ~150 km west of the lowest-latitude expanded craters mapped in the northern hemisphere, other than on isolated terrains (Viola & McEwen, 2018). We interpret the isolated mounds as inverted craters formed during ice loss (Figure S9 in Supporting Information S1): Aeolian material trapped within a crater slows sublimation there and remains as a mound after the surrounding ice sublimates deeper than the crater floor (Dundas et al., 2015). One alternative possibility that they are volcanic rootless cones (cf., Keszthelyi et al., 2010) can be ruled out because there is a gradational sequence with larger flat-topped

features (Figure 4c). The largest mound is ~200 m across. Taking this as a lower bound on the diameter of the former crater, at least ~30 m of ice (the depth of the crater floor below the original ground surface) has likely been lost. Similar mounds are found as far south as ~33°N but are not observed on the well-defined lava textures further equatorward (Figure S5 in Supporting Information S1), so either past massive ice did not extend below 33°N in the past, or the mounds erode quickly.

Remote-sensing data do not indicate abundant shallow ice in this region. Neutron spectrometer data indicate <15 wt% H_2O in the upper 50 cm of the subsurface at hundreds-of-km scales (Malakhov et al., 2020; Pathare et al., 2018), consistent with hydrated minerals or a small component of pore ice. Thermophysical ice detection with Mars Climate Sounder data has not been attempted here (Piqueux et al., 2019); Thermal Emission Spectrometer analysis (Sizemore et al., 2020) by the Subsurface Water Ice Mapping (SWIM) project did not reveal ice in the upper tens of cm. Shallow Radar surface reflection mapping by the SWIM project (Morgan et al., 2020) are consistent with ice in the upper 5 m of the subsurface.

Ice stability models show that this region is more favorable to low-latitude ground ice than other regions at this latitude, and that the exact position of the latitudinal boundary is particularly sensitive to recent climate conditions (Mellon et al., 2004). While ice is unstable here under a global-average atmospheric water abundance of 10 precipitable microns (pr. μm), typical of the era of spacecraft measurements (e.g., Montmessin et al., 2017), this region would have had stable ice if there were ≥20 pr. μm of atmospheric water vapor (Mellon et al., 2004), well within the range of predicted past variations. The current regional and global distribution of ice is consistent with the distribution that would be stable with a multi-kyr average of 26 pr. μm (Mellon & Sizemore, 2022).

5. Discussion

Our observations indicate patchy and/or deeply buried ice at this location. The blocks near the rim of the new crater indicate bodies of strong massive ice locally ≥3 m thick, buried or surrounded by some combination of unconsolidated regolith and pore-filling ice. Massive ice likely occurs at several meters depth and the depth and thickness may be variable. Flat-floored secondary craters suggest a shallow strong layer, likely pore ice cementing regolith grains at the ice table (i.e., the sharp boundary between ice-free regolith and icy permafrost). Such a boundary is the most likely explanation for a shallow strength transition given that shallow ice is present and that the depth to coherent rock is considerably greater. Thus, the massive ice exposed by the impact is likely overlain by pore ice beginning near 1 m depth. This ice table structure is broadly consistent with theoretical predictions for ice sheet retreat on Mars (e.g., Schorghofer, 2007; Schorghofer & Forget, 2012) but exists at a shallower depth and lower latitude than predicted.

We hypothesize that massive ice >30 m thick was once present, likely contiguous with the extant deposit to the northeast (Bramson et al., 2015). This layer likely formed by snow and frost accumulation as it is thicker than expected for other formation processes such as ice lens growth or thermal cycling-enhanced vapor diffusion (Fisher, 2005; Sizemore et al., 2015), although advection of perchlorate solution has been suggested to produce thick layers (Fisher et al., 2022). The equatorward limit of the surface ice was likely near 33°N, as candidate inverted craters are not seen below that latitude. Most of this massive ice appears to have sublimated. Loss would have occurred progressively, punctuated by stable intervals when pore ice formed (e.g., Mellon & Sizemore, 2022; Schorghofer, 2007; Schorghofer & Forget, 2012). The extensive ice loss marks a climate shift that destabilized the massive ice and drove net sublimation. Two plausible causes are a hypothesized transition in mean obliquity from ~36° to ~25° between 4 and 2.5 Ma or the end of an era of recent obliquity peaks near 30° at 380 ka (Laskar et al., 2004), each of which could reduce the average stability of surface and subsurface mid-latitude ice (Bramson et al., 2017; Mellon & Sizemore, 2022). Crater retention ages of mantle deposits elsewhere in the mid-latitudes suggest icy-mantle degradation timeframes consistent with the latter (Schon et al., 2012), but extensive deposition and sublimation here pose challenges for crater chronology. Stable intervals, both recent and at past higher obliquities, allowed deposition of pore ice within the sublimation lag (Mellon & Jakosky, 1995), sourced from the atmosphere or the deeper massive ice itself; the most recent period of stability would have ended 100–50 ka (Mellon & Sizemore, 2022). This pore ice has receded ~1 m since that time, as the equilibrium ice depth in this region is <1 cm when stable (Mellon et al., 2004; Mellon & Sizemore, 2022).

Our results constrain the past size and thickness of a Martian ice deposit. Climate oscillations must have occurred to emplace and partially remove pore ice above the massive ice, as monotonic ice loss would yield a desiccated

lag directly above such ice. Paleoclimate models predict mid-latitude surface ice accumulation above 35°–40°N at obliquities near 35°, or equatorial accumulation possibly reaching 35°N at 45° obliquity (Forget et al., 2006; Levrard et al., 2004; Madeleine et al., 2009, 2014; Mischna et al., 2003). Accumulation as part of a mid-latitude deposit is consistent with the nearby radar-inferred ice layer from 38° to 52°N (Bramson et al., 2015), and the lack of evidence for crater inversion equatorward of 33°N suggests that major accumulation of massive ice did not extend to lower latitudes. Hence, we favor ice deposition in this region at periods of ∼35° obliquity, while equatorial deposition at 40°–45° obliquity would have been localized geographically (Forget et al., 2006; Levrard et al., 2004; Madeleine et al., 2009). The new crater described herein is near the edge of or outside the accumulation region in many models (Forget et al., 2006; Levrard et al., 2004; Madeleine et al., 2009, 2014; Mischna et al., 2003).

Retreat of massive ice to >1 m depth here supports predictions that lower-latitude ice is either more deeply buried, or localized beneath pole-facing slopes (e.g., Aharonson & Schorghofer, 2006; Mellon & Sizemore, 2022). The coincidence of extant massive ice with some of the lowest-latitude expanded craters supports the hypothesis that those landforms indicate partial loss of massive ice, supporting their use to infer its presence elsewhere; expanded craters exist in certain geographic settings at latitudes as low as 25°N (Viola and McEwen (2018)). Our results provide fundamental constraints for paleoclimate models, including the depth and structure of ice near the survival limits of shallow ice. They will also inform future searches for lower-latitude ice across Mars, useful for future exploration.

Data Availability Statement

HiRISE data are available at https://doi.org/10.17189/1520303 and https://doi.org/10.17189/1520227 (McEwen, 2007, 2009). CTX data are available at https://doi.org/10.17189/1520266 (M. Malin, 2007), and CRISM data at https://doi.org/10.17189/1519507 (Murchie, 2007). SWIM ice consistency maps are available at https://swim.psi.edu/SWIM2Products.php (Morgan et al., 2020; Sizemore et al., 2020). Data for deconvolved two-layer neutron spectrometer maps is available via Pathare et al. (2018). The iSALE-2D code is available for academic use upon request at: https://isale-code.github.io (Collins et al., 2004; Wünnemann et al., 2006).

Acknowledgments

We thank the operations teams of MRO, HiRISE, CTX, and CRISM. This work was funded by the Mars Reconnaissance Orbiter Project, the InSight Project, NASA Grant 80NSSC20K0971 to IJD, Australian Research Council Grant FT210100063 to KM, and UK Science and Technology Facilities Council Grant ST/S000615/1 to GSC. LLT and VGR acknowledge funding and support from the Canadian NSERC Discovery Grant programme (RGPIN 2020-06418) and the Canadian Space Agency (CSA) Planetary and Astronomy Missions Co-Investigator programme (22EXPCOI3). A portion of the research described in this paper was done by the InSight Project, Jet Propulsion Laboratory, California Institute of Technology, under a contract with the National Aeronautics and Space Administration. Tim Haltigin and an anonymous reviewer provided helpful comments. We thank the developers of iSALE-2D, including Gareth Collins, Kai Wünnemann, Dirk Elbeshausen, Tom Davison, Boris Ivanov, and Jay Melosh. We thank Kris Akers for producing a HiRISE DTM. Any use of trade, firm, or product names is for descriptive purposes only and does not imply endorsement by the U.S. Government.

References

Aharonson, O., & Schorghofer, N. (2006). Subsurface ice on Mars with rough topography. *Journal of Geophysical Research*, *111*(E11), E11007. https://doi.org/10.1029/2005JE002636

Bart, G. D. (2014). The quantitative relationship between small impact crater morphology and regolith depth. *Icarus*, *235*, 130–135. https://doi.org/10.1016/j.icarus.2014.03.020

Boynton, W. V., Feldman, W. C., Squyres, S. W., Prettyman, T. H., Brückner, J., Evans, L. G., et al. (2002). Distribution of hydrogen in the near surface of Mars: Evidence for subsurface ice deposits. *Science*, *297*(5578), 81–85. https://doi.org/10.1126/science.1073722

Bramson, A. M., Byrne, S., & Bapst, J. (2017). Preservation of mid-latitude ice sheets on Mars. *Journal of Geophysical Research: Planets*, *122*(11), 2250–2266. https://doi.org/10.1002/2017JE005357

Bramson, A. M., Byrne, S., Putzig, N. E., Sutton, S., Plaut, J. J., Brothers, T. C., & Holt, J. W. (2015). Widespread excess ice in Arcadia Planitia, Mars. *Geophysical Research Letters*, *42*(16), 6566–6574. https://doi.org/10.1002/2015GL064844

Chamberlain, M. A., & Boynton, W. V. (2007). Response of Martian ground ice to orbit-induced climate change. *Journal of Geophysical Research*, *112*(E6), E06009. https://doi.org/10.1029/2006JE002801

Collins, G. S., Melosh, H. J., & Ivanov, B. A. (2004). Modeling damage and deformation in impact simulations. *Meteoritics & Planetary Sciences*, *39*(2), 217–231. https://doi.org/10.1111/j.1945-5100.2004.tb00337.x

Dundas, C. M., Byrne, S., & McEwen, A. S. (2015). Modeling the development of Martian sublimation thermokarst landforms. *Icarus*, *262*, 154–169. https://doi.org/10.1016/j.icarus.2015.07.033

Dundas, C. M., Byrne, S., McEwen, A. S., Mellon, M. T., Kennedy, M. R., Daubar, I. J., & Saper, L. (2014). HiRISE observations of new impact craters exposing Martian ground ice. *Journal of Geophysical Research: Planets*, *119*(1), 109–127. https://doi.org/10.1002/2013JE004482

Dundas, C. M., Mellon, M. T., Conway, S. J., Daubar, I. J., Williams, K. E., Ojha, L., et al. (2021). Widespread exposures of extensive clean shallow ice in the Martian mid-latitudes. *Journal of Geophysical Research: Planets*, *126*(3), e2020JE006617. https://doi.org/10.1029/2020JE006617

Durham, W. B., Heard, H. C., & Kirby, S. H. (1983). Experimental deformation of polycrystalline H_2O ice at high pressure and low temperature—Preliminary results. *Journal of Geophysical Research*, *88*(S01), B377–B392. https://doi.org/10.1029/JB088iS01p0B377

Fisher, D. A. (2005). A process to make massive ice in the Martian regolith using long-term diffusion and thermal cracking. *Icarus*, *179*(2), 387–397. https://doi.org/10.1016/j.icarus.2005.07.024

Fisher, D. A., Lacelle, D., & Pollard, W. (2022). A possible perchlorate-enabled mechanism for forming thick near surface excess ice layers; in the Amazonian regolith of Mars. *Icarus*, *387*, 115198. article #115198. https://doi.org/10.1016/j.icarus.2022.115198

Forget, F., Haberle, R. M., Montmessin, F., Levrard, B., & Head, J. W. (2006). Formation of glaciers on Mars by atmospheric precipitation at high obliquity. *Science*, *311*(5759), 368–371. https://doi.org/10.1126/science.1120335

Holt, J. W., Safaeinili, A., Plaut, J. J., Head, J. W., Phillips, R. J., Seu, R., et al. (2008). Radar sounding evidence for buried glaciers in the southern mid-latitudes of Mars. *Science*, *322*(5905), 1235–1238. https://doi.org/10.1126/science.1164246

Keszthelyi, L., Jaeger, W., McEwen, A., Tornabene, L., Beyer, R. A., Dundas, C., & Milazzo, M. (2008). High resolution imaging science experiment (HiRISE) images of volcanic terrains from the first 6 months of the Mars reconnaissance orbiter primary science phase. *Journal of Geophysical Research*, *113*(E4), E04005. https://doi.org/10.1029/2007JE002968

Keszthelyi, L. P., Jaeger, W., Dundas, C., Martinez-Alonso, S., McEwen, A., & Milazzo, M. (2010). Hydrovolcanic features on Mars: Preliminary observations from the first Mars year of HiRISE imaging. *Icarus*, *205*(1), 211–229. https://doi.org/10.1016/j.icarus.2009.08.020

Kreslavsky, M. A., & Head, J. W. (2002). Mars: Nature and evolution of young latitude-dependent water-rich mantle. *Geophysical Research Letters*, *29*(15), 1719. https://doi.org/10.1029/2002GL015392

Laskar, J., Correia, A. C. M., Gastineau, M., Joutel, F., Levrard, B., & Robutel, P. (2004). Long term evolution and chaotic diffusion of the insolation quantities of Mars. *Icarus*, *170*(2), 343–364. https://doi.org/10.1016/j.icarus.2004.04.005

Levrard, B., Forget, F., Montmessin, F., & Laskar, J. (2004). Recent ice-rich deposits formed at high latitudes on Mars by sublimation of unstable equatorial ice during low obliquity. *Nature*, *431*(7012), 1072–1075. https://doi.org/10.1038/nature03055

Madeleine, J.-B., Forget, F., Head, J. W., Levrard, B., Montmessin, F., & Millour, E. (2009). Amazonian northern mid-latitude glaciation on Mars: A proposed climate scenario. *Icarus*, *203*(2), 390–405. https://doi.org/10.1016/j.icarus.2009.04.037

Madeleine, J.-B., Head, J. W., Forget, F., Navarro, T., Millour, E., Spiga, A., et al. (2014). Recent Ice Ages on Mars: The role of radiatively active clouds and cloud microphysics. *Geophysical Research Letters*, *41*(14), 4873–4879. https://doi.org/10.1002/2014GL059861

Malakhov, A. V., Mitrofanov, I. G., Litvak, M. L., Sanin, A. B., Golovin, D. V., Djachkova, M. V., et al. (2020). Ice permafrost "oases" close to Martian equator: Planet neutron mapping based on data of FREND Instrument onboard TGO Orbiter of Russian-European ExoMars mission. *Astronomy Letters*, *46*(6), 407–421. https://doi.org/10.1134/S1063773720060079

Malin, M. (2007). MRO context camera experiment data record level 0 V1.0, MRO-M-CTX-2-EDR-L0-V1.0. *NASA Planetary Data System*. https://doi.org/10.17189/1520266

Malin, M. C., Bell, J. F., Cantor, B. A., Caplinger, M. A., Calvin, W. M., Clancy, R. T., et al. (2007). Context camera investigation on board the Mars reconnaissance orbiter. *Journal of Geophysical Research*, *112*(E5), E05S04. https://doi.org/10.1029/2006JE002808

McEwen, A. (2007). Mars reconnaissance orbiter high resolution imaging science experiment, reduced data record, MRO-M-HIRISE-3-RDR-V1.1. *NASA Planetary Data Syste*m. https://doi.org/10.17189/1520303

McEwen, A. (2009). Mars reconnaissance orbiter high resolution imaging science experiment, digital terrain model, MRO-M-HIRISE-5-DTM-V1.0. *NASA Planetary Data System*. https://doi.org/10.17189/1520227

McEwen, A. S., Eliason, E. M., Bergstrom, J. W., Bridges, N. T., Hansen, C. J., Delamere, W. A., et al. (2007). Mars reconnaissance orbiter's high resolution imaging science experiment (HiRISE). *Journal of Geophysical Research*, *112*(E5), E05S02. https://doi.org/10.1029/2005JE002605

Mellon, M. T., & Jakosky, B. M. (1995). The distribution and behavior of Martian ground ice during past and present epochs. *Journal of Geophysical Research*, *100*(E6), 11781–11799. https://doi.org/10.1029/95JE01027

Mellon, M. T., Feldman, W. C., & Prettyman, T. H. (2004). The presence and stability of ground ice in the southern hemisphere of Mars. *Icarus*, *169*(2), 324–340. https://doi.org/10.1016/j.icarus.2003.10.022

Mellon, M. T., & Sizemore, H. G. (2022). The history of ground ice at Jezero Crater Mars and other past, present, and future landing sites. *Icarus*, *371*, 114667. article #114667. https://doi.org/10.1016/j.icarus.2021.114667

Melosh, H. J. (1989). *Impact cratering: A geologic process*. Oxford University Press.

Mischna, M. A., Richardson, M. I., Wilson, R. J., & McCleese, D. J. (2003). On the orbital forcing of Martian water and CO_2 cycles: A general circulation model study with simplified volatile schemes. *Journal of Geophysical Research*, *108*(E6), 5062. https://doi.org/10.1029/2003JE002051

Montmessin, F., Smith, M. D., Yangevin, Y., Mellon, M. T., & Fedorova, A. (2017). The water cycle. In R. M. Haberle, R. T. Clancy, F. Forget, M. D. Smith, & R. W. Zurek (Eds.), *The atmosphere and climate of Mars* (pp. 338–373). Cambridge. https://doi.org/10.1017/9781139060172.011

Morgan, G. A., Putzig, N. E., Campbell, B. A., Bain, Z. M., Bramson, A. M., Petersen, E. I., et al. (2020). Subsurface water ice mapping (SWIM) on Mars: Radar surface reflectivity. In *Lunar and planetary science conference*, (Vol. *51*). abstract #2790.

Murchie, S. (2007). Mars reconnaissance orbiter compact reconnaissance imaging spectrometer for Mars experiment data record, MRO-M-CRISM-2-EDR-V1.0. *NASA Planetary Data System*. https://doi.org/10.17189/1519507

Murchie, S., Arvidson, R., Bedini, P., Beisser, K., Bibring, J. P., Bishop, J., et al. (2007). Compact reconnaissance imaging spectrometer for Mars (CRISM) on Mars reconnaissance orbiter (MRO). *Journal of Geophysical Research*, *112*(E5), E05S03. https://doi.org/10.1029/2006JE002682

Pathare, A. V., Feldman, W. C., Prettyman, T. H., & Maurice, S. (2018). Driven by excess? Climatic implications of new global mapping of near-surface water-equivalent hydrogen on Mars. *Icarus*, *301*, 97–116. https://doi.org/10.1016/j.icarus.2017.09.031

Pierazzo, E., Vickery, A. M., & Melosh, H. J. (1997). A reevaluation of impact melt production. *Icarus*, *127*(2), 408–423. https://doi.org/10.1006/icar.1997.5713

Pike, R. J., & Wilhelms, D. E. (1978). Secondary-impact craters on the Moon: Topographic form and geologic process. *LPSC*, *9*, 907–909.

Piqueux, S., Buz, J., Edwards, C. S., Bandfield, J. L., Kleinböhl, A., Kass, D. M., et al. (2019). Widespread shallow water ice on Mars at high latitudes and mid latitudes. *Geophysical Research Letters*, *46*(24), 14290–14298. https://doi.org/10.1029/2019GL083947

Posiolova, L. V., Lognonne, P., Banerdt, W. B., Clinton, J., Collins, G. S., Kawamura, T., et al. (2022). Large recent impact craters on Mars: Orbital imagery and surface seismic co-investigation. *Science*, *378*(6618), 412–417. https://doi.org/10.1126/science.abq7704

Quaide, W. L., & Oberbeck, V. R. (1968). Thickness determination of the lunar surface layer from lunar impact craters. *Journal of Geophysical Research*, *73*(16), 5247–5270. https://doi.org/10.1029/JB073i016p05247

Rajšić, A., Miljković, K., Wójcicka, N., Collins, G. S., Onodera, K., Kawamura, T., et al. (2021). Numerical simulations of the Apollo S-IVB artificial impacts on the Moon. *Earth and Space Science*, *8*(12), e2021EA001887. https://doi.org/10.1029/2021EA001887

Schon, S. C., Head, J. W., & Fassett, C. I. (2012). Recent high-latitude resurfacing by a climate-related latitude-dependent mantle: Constraining age of emplacement from counts of small craters. *Planetary and Space Science*, *69*(1), 49–61. https://doi.org/10.1016/j.pss.2012.03.015

Schorghofer, N. (2007). Dynamics of ice ages on Mars. *Nature*, *449*(7159), 192–195. https://doi.org/10.1038/nature06082

Schorghofer, N., & Forget, F. (2012). History and anatomy of subsurface ice on Mars. *Icarus*, *220*(2), 1112–1120. https://doi.org/10.1016/j.icarus.2012.07.003

Shaw, A., Arvidson, R. E., Bonitz, R., Carsten, J., Keller, H. U., Lemmon, M. T., et al. (2009). Phoenix soil physical properties investigation. *Journal of Geophysical Research*, *114*, E00E05. https://doi.org/10.1029/2009JE003455

Sizemore, H. G., Pathare, A., Dundas, C. M., Putzig, N. E., Courville, S. W., Perry, M., et al. (2020). Shallow ice detection on Mars: Integration of thermal and neutron datasets into the Mars Subsurface Water Ice Mapping (SWIM) project. In *AGU fall meeting*. abstract #P055-0004.

Sizemore, H. G., Zent, A. P., & Rempel, A. W. (2015). Initiation and growth of Martian ice lenses. *Icarus*, *251*, 191–210. https://doi.org/10.1016/j.icarus.2014.04.013

Smith, P. H., Tamppari, L. K., Arvidson, R. E., Bass, D., Blaney, D., Boynton, W. V., et al. (2009). H2O at the Phoenix landing site. *Science*, *325*(5936), 58–61. https://doi.org/10.1126/science.1172339

Tanaka, K. L., Skinner, J. A., Dohm, J. M., Irwin, R. P., Kolb, E. J., Fortezzo, C. M., et al. (2014). Geologic map of Mars. *United States Geological Survey Scientific Investigations Map*, *3292*. https://doi.org/10.3133/sim3292

Viola, D., & McEwen, A. S. (2018). Geomorphological evidence for shallow ice in the southern hemisphere of Mars. *Geophysical Research Letters*, *123*(1), 262–277. https://doi.org/10.1002/2017JE005366

Wünnemann, K., Collins, G. S., & Melosh, H. J. (2006). A strain-based model for use in hydrocode simulations of impacts and implications for transient crater growth in porous targets. *Icarus*, *180*(2), 514–527. https://doi.org/10.1016/j.icarus.2005.10.013

References From the Supporting Information

Morgan, F., Mustard, J. F., Wiseman, S. M., Seelos, F. P., Murchie, S. L., McGuire, P. C., & CRISM team. (2011). Improved algorithm for CRISM volcano scan atmospheric correction. In *42nd annual lunar and planetary science conference*, (Vol. *42*). abstract #2453.

Morgan, G. A., Putzig, N. E., Perry, M. R., Sizemore, H. G., Bramson, A. M., Petersen, E. I., et al. (2021). Availability of subsurface water-ice resources in the northern mid-latitudes of Mars. *Nature Astronomy*, *5*(3), 230–236. https://doi.org/10.1038/s41550-020-01290-z